ORGANOMETALLICS

pubs.acs.org/Organometallics Article

Electronic Effects of Aminoindenyl Ligands Coordinated to Manganese: Structures and Properties of a Mn⁰ Metalloradical and Bimetallic Mn⁻¹/Mn¹ Adduct

David S. Tresp, Hagen Neugebauer, Stefan Grimme, Andreas Hansen,* and Demyan E. Prokopchuk*



Cite This: https://doi.org/10.1021/acs.organomet.2c00463



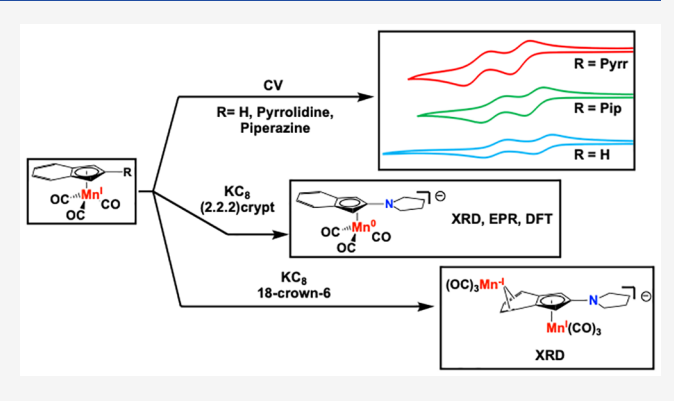
ACCESS I

III Metrics & More

Article Recommendations

s Supporting Information

ABSTRACT: Studying the redox behavior of Earth-abundant metal complexes and understanding their reactivity under reducing conditions is of fundamental importance for activating small molecules. We present the electrochemical behavior and reactivity of amine-functionalized indenylmanganese(I) complexes that form the piano-stool complexes $\mathrm{Mn^I(CO)_3(Ind^R)}$ (R = pyrrolidinyl, piperazinyl), which exhibit two cathodic redox waves via cyclic voltammetry (CV). Electrochemical, spectroscopic, and structural comparisons of these complexes with undecorated indenyl species reveal that the pyrrolidine-substituted tricarbonylmanganese complex $\mathrm{MnInd}^{\mathrm{Pyrr}}$ is the most electron-rich due to favorable π -donor effects from the amine to the ring system. These results are also strongly supported by DFT computations. Although CV



studies show clean redox behavior, reaction outcomes in the presence of common chemical reductants are strongly dependent on the reagents used. The reduction of MnInd^{Pyrr} with KC₈ in the presence of the encapsulating agent 2,2,2-Crypt led to the formation of a rare Mn⁰ metalloradical, $[K(2,2,2-\text{Crypt})][\text{MnInd}^{Pyrr}]$, which was characterized by single-crystal X-ray diffraction, EPR spectroscopy, IR spectroscopy, and DFT calculations. Attempts to isolate a doubly reduced Mn^{-I} adduct in the presence of 18-crown-6 resulted in indenide anion loss that generated a mixed-valence Mn^{-I}/Mn^I adduct, where the two metal centers were bound to a single indenyl moiety. This study emphasizes the dramatic differences between observing redox-reversible behavior on the electroanalytical scale and performing preparative-scale reduction reactions with alkali metals and encapsulating agents, as these reagents have a profound impact on the reaction outcome.

■ INTRODUCTION

Piano-stool complexes containing Earth-abundant metals and cyclopentadienyl (Cp) or indenyl (Ind) ligands have attracted renewed interest for small-molecule activation in recent years due to their redox stability and role as electrocatalysts in the reduction of protons to hydrogen and carbon dioxide to formic acid. 1-7 Under oxidative conditions, the indenyl group has also been identified as a "non-innocent" ligand at iron. It triggers an $\eta^5 - \eta^6$ hapticity shift coupled with metal hydride migration to the η^5 -Cp ring, yielding a complex with very weak homolytic C-H bond strength. We recently reported that protonation at the carbon atom on the Cp ring is thermodynamically favored during H2 production electrocatalysis, even in the presence of pendant amines directly attached to Cp.5 These counterintuitive findings suggest that amine-functionalized M(Cp) and M(Ind) complexes may exhibit chemically "non-innocent" reactivity that remains underexplored for small-molecule activation under positive or negative electrical bias.

It is known that tricarbonyl piano-stool complexes $M(Cp^R)$ - $(CO)_3$ and $M(Ind^R)(CO)_3$ (M = Mn, Fe) exhibit divergent electrochemical activity. The oxidation of cymantrenes

 $(Cp^RMn(CO)_3)$ has been studied as a function of the Cp ring substitution pattern (R = H, NH₂, Me₅) to generate stable radical cations. However, the cathodic electrochemistry of $CpMn(CO)_3$ reveals a very negative and irreversible single-electron reduction (-2.9 V vs $Fc^{+/0}$, THF). In contrast, isostructural $IndMn(CO)_3$ has two cathodic and electrochemically reversible redox couples (-2.3 V and -2.5 V vs $Fc^{+/0}$, THF); the stability of these anions suggests that the CO ligands remain coordinated to Mn and an $\eta^5 - \eta^3$ haptotropic shift (i.e., ring slippage) becomes important to accommodate the influx of electrons after the second reduction event. Evidence for $[IndMn(CO)_3]^-$ and $[IndMn(CO)_3]^{2-}$ was only reported based on solution-phase spectroscopic data and reactivity studies. With iron, The $1e^-$ reduction of

Received: September 10, 2022



isostructural IndFe(CO)₃⁺ results in CO release, with the CO dissociation rate constant being 10^6 slower than that for the corresponding CpFe(CO)₃⁺ complex.¹³ This observation was coined an "inverse indenyl effect" from DFT calculations, where a π^* LUMO on the indenyl benzene ring generates a ligand-based radical that tempers ligand dissociations at Fe.

Our group is interested in preparing amine-functionalized Cp ligands to understand their electronic and secondary coordination-sphere effects in electrocatalytic reactions involving protons and electrons,⁵ and we now report the reactivity of amine complexes $Mn(Ind^R)(CO)_3$ (R = pyrrolidinyl, piperazinyl) under reducing conditions. Electrochemical studies of $Mn(Ind^R)(CO)_3$ in the cathodic direction reveal two reversible redox events, with DFT calculations, IR spectra, and molecular structures revealing a correlation between the CO stretching frequency and the π -donor ability of the amine to the indenyl ring. One-electron reduction of Mn(Ind^{Pyrr})(CO)₃ with KC₈ in the presence of (2,2,2)-crypt generated a rare Mn⁰ metalloradical with a partial ring slip character, which was characterized by single-crystal X-ray diffraction and EPR spectroscopy. Conversely, the reduction of Mn(Ind^{Pyrr})(CO)₃ with KC₈ followed by the addition of 18-crown-6 results in indenide ligand loss and the formation of a bimetallic mixedvalent Mn^I/Mn^{-I} adduct that coordinates to a single Ind^{Pyrr} ligand. These results starkly contrast with the "clean" redox behavior via cyclic voltammetry, underscoring the involvement of alkali metals and encapsulating agents during reduction reactions with manganese piano-stool complexes.

■ RESULTS AND DISCUSSION

The amine-functionalized indene ligands $\operatorname{Ind}^{\operatorname{Pyrr}}H$ and $\operatorname{Ind}^{\operatorname{Pip}}H$ are easily synthesized via condensation by reacting the corresponding secondary amines with 2-indanone, resulting in air-stable and conveniently handled solids. The procedures for synthesizing piano-stool tricarbonyl complexes $\operatorname{MnInd}^{\operatorname{Pyrr}}$, $\operatorname{MnInd}^{\operatorname{Pip}}$, and $\operatorname{MnInd}^{\operatorname{15}}$ are all similar, where the first step involves the in situ generation of the indenide via a strong base (n-BuLi for $\operatorname{MnInd}^{\operatorname{Pyrr}}$ and $\operatorname{MnInd}^{\operatorname{Pip}}$) or reductant (Na^0 for MnInd), followed by the addition of $\operatorname{Mn}(\operatorname{CO})_5\operatorname{Br}$ or $\operatorname{Mn}(\operatorname{CO})_3(\operatorname{py})_2\operatorname{Br}$ to generate the indenylmanganese complexes (Scheme 1). The new indenyl complex in this triad is

Scheme 1. General Synthetic Protocol for Preparing MnInd $^{\rm Pyrr}$, MnInd $^{\rm Pip}$, $^{\rm 14}$ and MnInd $^{\rm 15}$

M = Li, Na R= Pyrr, Pip, H

MnInd^{Pyrr}, an air-stable solid purified by silica gel column chromatography. This initially elutes $Mn_2(CO)_{10}$ as a yellow band, followed by the dark orange MnInd^{Pyrr}, indicating that either indenide or *n*BuLi may behave as a reductant to convert $Mn(CO)_5$ Br to $Mn_2(CO)_{10}$ and explaining the relatively poor yield of the target compound (26%). MnInd^{Pyrr}, MnInd^{Pip} and MnInd all exhibit characteristic carbonyl IR frequencies that

demonstrate the electron-donating effect of the amine substituent on the ligand (or lack thereof), as shown in Table 1. Based on the experimental CO stretching frequencies, the order of the ligand donor strength is $Ind^{Pyrr} > Ind^{Pip} > Ind.$ DFT 17 frequency calculations of the complexes in acetonitrile $(\omega B97X-V^{18}/def2-TZVP+COSMO(MeCN)^{19,20})$ support this trend, and values are reported in parentheses in Table 1.

Single crystals of MnInd^{Pyrr} were grown by cooling a concentrated pentane solution of the complex (Figure 1). A structural comparison between MnInd^{Pyrr} and the known MnInd^{Pip14} reveals short C–N bond lengths (1.360(2) and 1.368(4)–1.378(4) Å, ¹⁴ respectively) that are on the order of a C=N double bond (average aromatic C=N bond length is 1.336 Å²¹). The dihedral angle between the appended amine and the Cp fragment becomes more planar as the electron donation from the amine increases, forcing the nitrogen into the same plane as the Cp ring (Table 1). These structural data are consistent with the CO stretching frequency data, where the smallest dihedral angle found for the pyrrolidine-appended ligand represents the most electron-donating ligand in the series (Table 1).

Cymantrene (CpMn(CO)₃) has an irreversible reduction potential of -2.9 V vs $Fc^{+/0}$ in acetonitrile, generating a formally 19e complex. According to DFT calculations, the electrons populate an antibonding ligand MO, 22,23 resulting in proposed Cp ring slippage from η^5 to η^3 . Cyclic voltammograms (CVs) recorded under N2 show that these indenyl complexes have two reversible redox waves centered at ca. -2.3 and -2.5 V (Figure 2). If the potential window for CV is swept too positive (> -1 V), the current response of the second reduction decreases with repeated scans, which may be caused by oxidative degradation that passivates the electrode surface (Figures S1 and S2). In accordance with the IR evidence, the reduction potentials are correlated with the electron-donor capabilities of the indenyl ligand series, where MnInd^{Pyrr} > MnInd^{Pip} > MnInd (Figure 2). The reduction potentials computed with OT-ωB97X-V/ma-def2-QZVPP +COSMO-RS(MeCN), ²⁴⁻²⁶ shown in parentheses in Table 1, are also in excellent agreement with the experimental values. The DFT geometries of MnInd^{Pyrr} and the reduced species, shown in Figure 3, show that the first reduction generates a metalloradical, which we describe as having "partial ring slip", with the Cp ring coordinating somewhere in between η^5 and η^3 . Upon a second reduction, the DFT-calculated geometry distorts fully to an η^3 -configuration.

A previous report studied the reduction chemistry of the undecorated indenyl complex MnInd, with magnetic susceptibility measurements, reactivity studies, and EPR spectroscopy supporting the formation of [MnInd]⁻; however, its molecular structure remained elusive. 12 In our hands, MnIndPyrr can be reduced by one electron to the corresponding Mn⁰ anion $[K(2,2,2-Crypt)][MnInd^{Pyrr}]$ by the dropwise addition of 1.1 equiv of KC₈ suspended in THF into a stirred solution of MnInd^{Pyrr} and 2,2,2-Crypt at room temperature (Scheme 2). After workup, this highly sensitive compound was crystallized via vapor diffusion of pentane into a concentrated THF solution, consistently resulting in the cocrystallization of $[MnInd^{p_{yrr}}]^-$ and $[K(2,2,2-Crypt)][Mn(CO)_5]$ in 36% and 31% yields, respectively, as determined by elemental analysis of the recrystallized bulk product. Unfortunately, all attempts to separate these compounds via washing or recrystallization were unsuccessful due to their extremely similar solubility characteristics. Fortunately, both the dark green Mn⁰ and colorless Mn⁻¹

Table 1. Comparison of Selected Redox Events, IR Stretching Frequencies, and Structural Data a,b

complex	$E_{1/2}$ Red 1 (V vs Fc ^{+/0})	$E_{1/2}$ Red 2 (V vs Fc ^{+/0})	νCO (cm ⁻¹ , KBr)	dihedral angle $(^{\circ})$	C-N bond length (Å)
MnInd ^{Pyrr}	-2.34	-2.55	1990, 1899	6.9(1)	1.360(2)
	(-2.23)	(-2.58)	(1986, 1896)	(7.02)	(1.359)
$\mathbf{MnInd}^{\mathbf{Pip}}$	-2.27	-2.47	2006, 1907	$10.0(3) - 12.3(3)^{14}$	$1.368(4) - 1.378(4)^{14}$
	(-2.20)	(-2.55)	(1987, 1896)	(9.38)	(1.378)
MnInd	-2.23^{12}	-2.46^{12}	2018, 1929 ¹²		
	(-2.08)	(-2.37)	(1995, 1906)		
$[\mathbf{MnInd}^{\mathrm{Pyrr}}]^{-}$			1884, 1807, 1784	14.3(4)	1.380(5)
				(11.1)	(1.371)
$[\mathbf{Mn_2Ind^{Pyrr}}]^-$			1973, 1942, 1857, 1832	8.5(4)	1.380(5)

^aComputed data are shown in parentheses below the experimental data (see DFT Calculations for details). DFT IR frequencies are not shown for the anionic compounds due to their complicated electronic structures. ^bThe dihedral angles are described as the acute angles between the planes N1–C5–C6 and C5–C6–C7, see Figure 1.

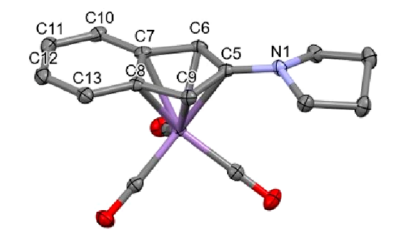


Figure 1. Molecular structure of MnInd^{Pyrr} with 50% probability ellipsoids. The dihedral angles in Table 1 are described as the acute angle between the planes N1-C5-C6 and C5-C6-C7.

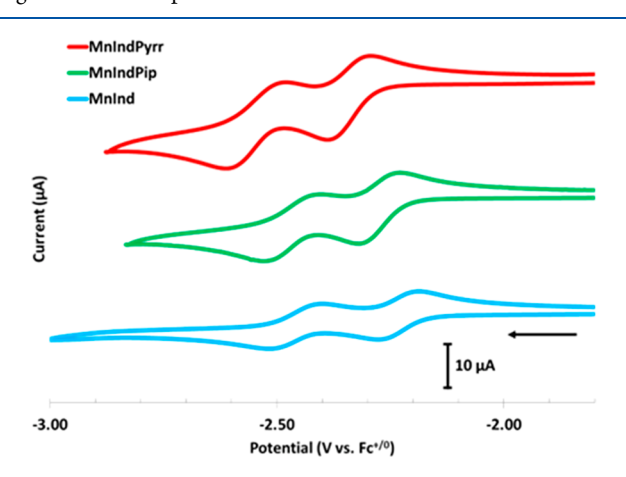


Figure 2. Stacked cyclic voltammograms of 1 mM solutions of MnInd^{Pyrr} (red), MnInd^{Pip} (green), and MnInd (blue) at 100 mV/s with 0.1 M [nBu_4N][PF $_6$] as the supporting electrolyte in MeCN. All CVs are referenced to Fc $^{+/0}$.

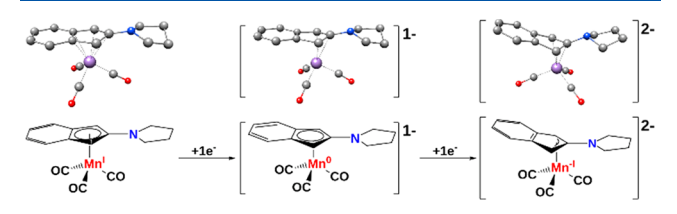
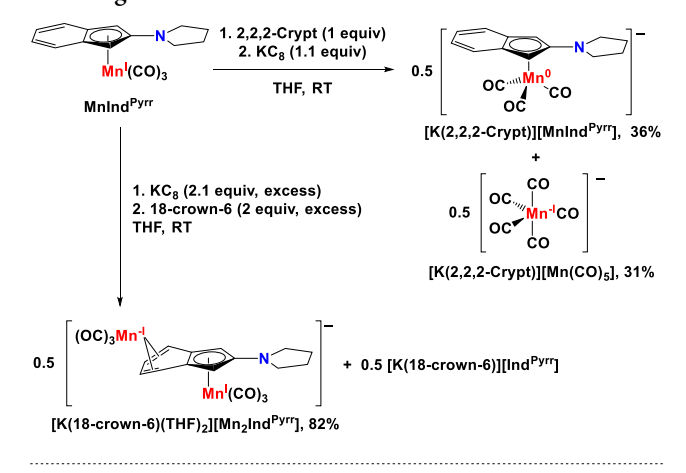
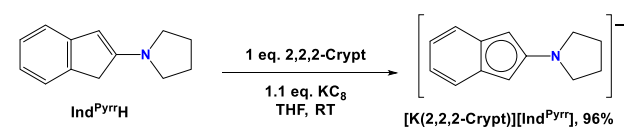


Figure 3. (Top) DFT geometries of MnInd^{Pyrr} optimized at the ω B97X-V/def2-TZVP+COSMO(MeCN) level of theory. Hydrogen atoms are omitted for clarity. (Bottom) Drawings of each product showing the subtle movement of the ligand from a partial ring slip orientation (middle) to full η^3 -coordination (right).

crystals are easily hand-picked for molecular structure determination by single-crystal X-ray diffraction (Figures 4 and S3). Evidence for the formation of [K(2,2,2-Crypt)][Mn-

Scheme 2. Reactivity of MnInd^{Pyrr} and Ind^{Pyrr}H under Reducing Conditions





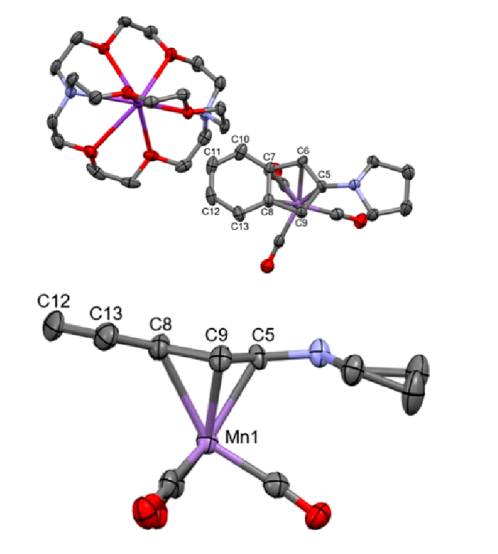


Figure 4. T(Top) Molecular structure of [K(2,2,2-Crypt)]- $[MnInd^{Pyrr}]$ with 50% probability ellipsoids. Hydrogens are omitted for clarity. (Bottom) Side-on view of $[MnInd^{Pyrr}]$ - showing the broken planarity of the five-membered ring.

 $(CO)_5$] is also supported by the CO stretching frequencies of $[Mn(CO)_5]^-$ in the FTIR spectrum.²⁷ Solution-phase ⁵⁵Mn NMR spectra of the cocrystallized mixture in THF- d_8 exhibited a characteristic ⁵⁵Mn NMR signal for $[Mn(CO)_5]^-$ at -2691 ppm²⁸ along with a second peak at -2919 ppm (Figure S8), which we speculate to be the dianion $[MnInd^{Pyrr}]^{2-}$ that we have been unable isolate or characterize any further.

The molecular structure of $[K(2,2,2-Crypt)][MnInd^{Pyrr}]$ is shown in Figure 4. Notably, structurally characterized monometallic Mn⁰ metalloradicals remain very rare and typically require significant steric protection to avoid dimerization. 29-33 Structural analysis shows that the [K-(2,2,2-Crypt)][MnInd^{Pyrr}] complex does not fully represent an indenyl ring slip to a standard η^3 -indenyl configuration, but 1e reduction certainly introduces structural distortions to the system. The C-N bond slightly elongates from 1.360(2) Å to 1.380(5) Å, which correlates well with the DFT-computed value (1.371 Å; Table 1). The dihedral angle increases from $6.9(1)^{\circ}$ to $14.3(4)^{\circ}$ (DFT value of 11.1°), which would be expected due to the increase in electronic repulsion with the presence of an additional electron. Interestingly, the ring slippage appears somewhere between an η^3 - and η^5 -indenyl configuration, where the ring has broken planarity but the C-C bond lengths for atoms C5 through C13 are nearly unchanged between MnIndPyrr and [MnIndPyrr]-, suggesting that the ring aromaticity is preserved (Table 2). The most

Table 2. - Comparison of C-C and Mn-C Bond Length Data (Å) for [MnInd^{Pyrr}] and [MnInd^{Pyrr}]

ato	m 1 a	tom 2	[MnInd ^{Pyrr}] (Å)	$[MnInd^{Pyrr}]^-$ (Å)
C	5	C6	1.428(2)	1.426(6)
Co	5	C7	1.440(2)	1.445(6)
C	7	C8	1.436(2)	1.428(7)
C	3	C9	1.437(2)	1.448(6)
C)	C5	1.437(2)	1.420(5)
C	7	C10	1.427(2)	1.395(7)
C	10	C11	1.359(2)	1.383(7)
C	11	C12	1.430(3)	1.392(8)
C	12	C13	1.367(2)	1.388(7)
C	13	C8	1.428(2)	1.403(6)
M	n1	C7	2.167(1)	2.472(5)
M	n1	C8	2.180(1)	2.471(5)
M	n1	C9	2.159(1)	2.201(4)
M	n1	C5	2.249(1)	2.200(4)
M	n1	C6	2.146(1)	2.195(5)

dramatic changes occur in the bond lengths between the Mn center and the carbons of the fused six-membered and Cp rings (Mn1–C7 and Mn1–C8), which elongate by ca. 0.30 Å upon reduction from MnInd^{Pyrr} to [MnInd^{Pyrr}]⁻. These elongations correlate well with the DFT-computed values of ca. 0.33 Å for the complex solvated in acetonitrile.

The X-band EPR spectrum of $[K(2,2,2\text{-Crypt})][\text{MnInd}^{\text{Pyrr}}]$ in 2-MeTHF glass at 77 K is shown in Figure 5. DFT calculations indicate that the residual unpaired spin density is located mainly at the Mn center, with small residual spin density on the six-membered ring of the indenyl ligand and the carbonyl ligands (Figure 5, bottom left). A best fit is achieved in the simulated EPR spectrum when 80% of the spectrum is attributed to a ⁵⁵Mn-centered radical (g = 1.997, 1.968, and 2.000) and 20% of the spectrum attributed to a second very similar ⁵⁵Mn center (g = 1.996, 1.977, and 2.007). The sum of

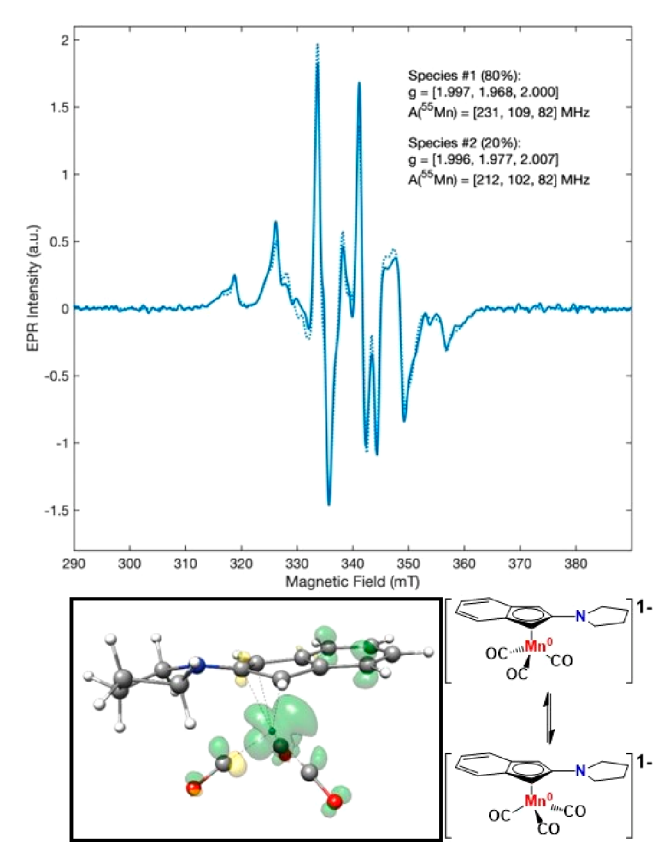


Figure 5. (Top) Experimental (solid line) and simulated (dotted line) X-band EPR spectra of $[K(2,2,2\text{-Crypt})][MnInd^{Pyrr}]$ in 2-MeTHF, including *g*-values and hyperfine tensors (*A*) for both ⁵⁵Mn centers. (Bottom) Computed residual spin density of $[MnInd^{Pyrr}]^-$ (isosurface value of 0.005 e Bohr^{-1/2}) and its proposed conformers in the EPR sample.

these contributions is shown in Figure 5 as the dotted line. Based on the extremely similar g-values and coupling constants for these two complexes, we suggest that two energetically similar conformers of [MnInd Pyrr] – exist in the glass, where the indenyl ligand ring is rotated relative to the three CO ligands of the piano-stool base (Figure 5, bottom right). This behavior has some precedent, as low-spin [CpMnII(CO)₂(IMes)][BF₄] was found to have two different g_3 values, which were ascribed to either two conformations in frozen solution or positional differences between the cation and the counteranion. However, in our case, we also cannot exclude the possibility of other another EPR-active molecule contaminating the sample.

Since these indenyl complexes exhibited two reversible redox events on the CV time scale, the chemical reduction of MnInd $^{\mathrm{Pyrr}}$ with more than one equivalent of KC₈ was explored (Scheme 2). The room-temperature addition of a THF suspension of a twofold excess of KC₈ to a solution of MnInd $^{\mathrm{Pyrr}}$ in THF under an N₂ atmosphere before the addition of an encapsulating agent resulted in the immediate formation of suspended graphite (C₈) and solution darkening. Next, the solution was treated with a twofold excess of 18-crown-6, filtered through Celite, and a red-orange oil was obtained after solvent removal. This solution was crystallized via pentane vapor diffusion into a THF solution at -35 °C, and single-crystal X-ray diffraction revealed the unusual bimetallic mixed-valent manganese complex [K(18-crown-6)(THF)₂]-[Mn₂Ind $^{\mathrm{Pyrr}}$] (Figure 6) with the loss of an indenide anion

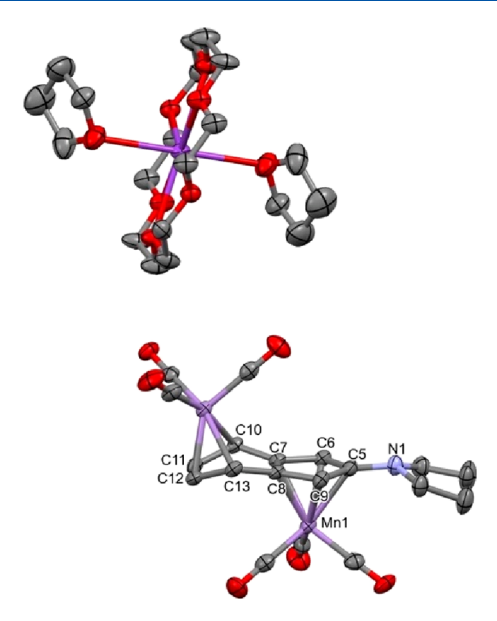


Figure 6. Molecular structures of $[K(18\text{-crown-6})(THF)_2]$ - $[Mn_2Ind^{Pyrr}]$ with 50% probability ellipsoids. Hydrogens and disordered THF are omitted for clarity.

(Scheme 2, bottom). Although additional characterization via 1 H NMR spectroscopy was achieved, separation to yield an analytically pure product proved challenging, which will be described in detail later. To the best of our knowledge, there are no other structurally authenticated group 7 compounds that form similar bimetallic structural motifs sharing a single indene ligand. Expanding a CCDC structural search to group 8 metals reveals a bimetallic "double decker" Ru complex, where a CpRu $^{\rm II}$ moiety coordinates to the $\eta^{\rm S}$ -Cp face of indene and a Cp*Ru $^{\rm II}$ moiety coordinates to the $\eta^{\rm G}$ -arene ring of indene. 35

To verify the stability of the indenide anion that is released upon the formation of $[K(18\text{-crown-6})(THF)_2][Mn_2Ind^{Pyrr}]$, free ligand $Ind^{Pyrr}H$ was directly reacted with KC_8 and (2,2,2)-crypt in THF to generate $[K(2,2,2)\text{-crypt}][Ind^{Pyrr}]$ (Scheme 2, bottom). Concentrating and cooling the reaction solution resulted in the crystallization of the analytically pure product in a 96% yield. The obtained crystals were suitable for single-crystal X-ray diffraction (SCXRD, Figure S4), and the free indenide was structurally distinct from the coordinated ligand. The C–N bond length is 1.381(8) Å, and the indenyl ring is nearly planar with a dihedral angle of $0.2(4)^{\circ}$. H NMR spectra support the planarization of this molecule, where the protons of the six-membered ring generate a symmetric AA'BB' splitting pattern (Figure S9).

After MnInd^{Pyrr} was reduced with 2.1 equiv of KC₈ and 2 equiv of 18-crown-6 was added to the reaction mixture, ¹H NMR spectra of the reduction mixture in THF-d₈ recorded after the mixture was washed with diethyl ether to remove traces of Ind^{Pyrr}H show a clean mixture of [Mn₂Ind^{Pyrr}]⁻ and [Ind^{Pyrr}]⁻ (Figure S13). Due to the incredibly similar solubility profiles of the reduction products, the yield of [Mn₂Ind^{Pyrr}]⁻ (82%) was determined by ¹H NMR spectroscopy of the crude reaction mixture, with addition of 1,3,5-trimethoxybenzene as an internal standard (Figure S11). Furthermore, [Mn₂Ind^{Pyrr}]⁻ is partly soluble in diethyl ether, and cooling a concentrated solution of this mixture for several days at -35 °C led to the crystallization of milligram quantities of X-ray-quality crystals of the bimetallic complex [K(18-crown-6)][Mn₂Ind^{Pyrr}] without THF coordinated to 18-crown-6 in the crystal lattice

(Figure 7). This result emphasizes the dynamic solvation—desolvation behavior of this complex, which further compli-

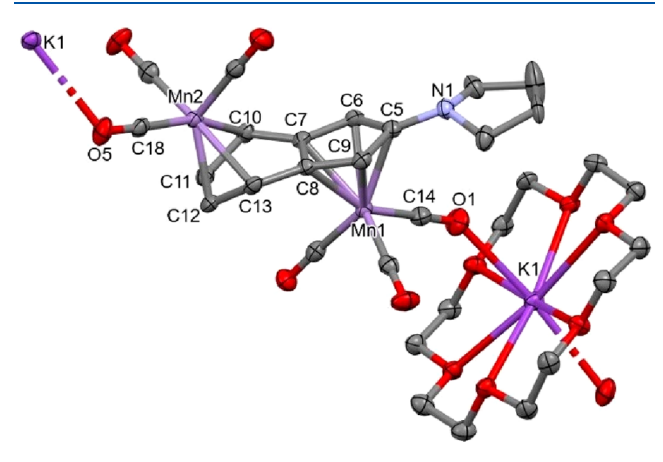
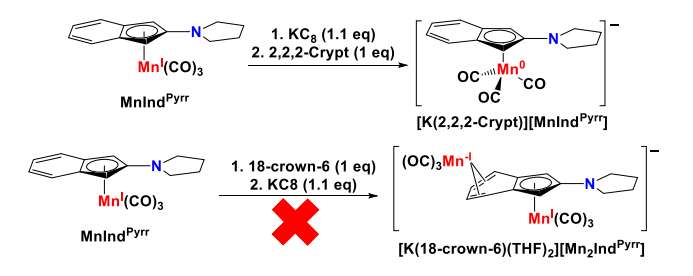


Figure 7. Molecular structure of $[K(18\text{-crown-6})][Mn_2Ind^{Pyrr}]$ with 50% probability ellipsoids. Hydrogens and disorder in the pyrrolidine ring are omitted for clarity.

cates isolation efforts to obtain high quantities of analytically pure product. The axial sites of potassium act as bridges between the Mn^ICO and Mn^{-I}CO moieties, weakly coordinating to the oxygen atoms of the bound CO ligands and forming an infinite chain in the crystal lattice. The Mn^ICO-K contact distance is 2.752(4) Å (O1-K1), and the Mn-ICO-K contact distance is 2.810(3) Å (O5-K1). In both the THFcoordinated and solvent-free structures, the Mn-coordinated C=C bonds are lengthened from an average C-C bond of 1.364 Å in the parent MnInd^{Pyrr} to average distances of 1.434 and 1.432 Å, respectively. In addition, Mn coordination to these alkenes dramatically alters their ¹H NMR chemical shifts, which change from 7.44 and 7.01 ppm in MnInd^{Pyrr} to 5.80 and 1.88 ppm in $[Mn_2Ind^{Pyrr}]^-$. The ¹H NMR spectrum of $[K(18\text{-crown-6})][Mn_2Ind^{Pyrr}]$ is shown in Figure S12, confirming the peak assignments of the reaction mixture described above. Therefore, we are confident that this novel bimetallic species reliably forms under conditions where reductant is added before 18-crown-6.

As illustrated in Scheme 2, the order of addition (reducing agent vs encapsulating agent) and the choice of encapsulating agent (2,2,2-Crypt vs 18-crown-6) are important for the reaction outcome. Scheme 3 summarizes the results of other permutations not discussed in Scheme 2. Adding KC₈ before 2,2,2-crypt yields a dark green solution, qualitatively indicating that the formation of $[K(2,2,2-Crypt)][MnInd^{Pyrr}]$ is not dependent on the reagent order when 2,2,2-Crypt is used. Adding 18-crown-6 before KC₈ generates an intractable mixture

Scheme 3. Reactivity of MnInd^{Pyrr} with Different Encapsulating Reagents and Orders of Addition



instead of $[K(18\text{-crown-6})(THF)_2][Mn_2Ind^{Pyrr}]$, clearly indicating that the order of addition is essential when using 18-crown-6. Work-up of a reaction mixture containing single equivalents of both KC_8 and 18-crown-6 did not result in a clean mixture of $[K(18\text{-crown-6})][Mn_2Ind^{Pyrr}]$ and $[K(18\text{-crown-6})][Ind^{Pyrr}]$, which required the use of a twofold excess of the reductant and the encapsulating agent, as shown in Scheme 2.

CONCLUSIONS

We have explored the cathodic electrochemistry and reactivity of aminoindenyl manganese tricarbonyl complexes. The deviations in planarity between the amine and the Cp ring in the solid state dictate the observed electrochemical and spectroscopic signatures in solution. Increased ligand planarity results in greater π -electron donation from the amine to the Cp ring, boosting the electron density at Mn. The structural, electrochemical, and IR spectroscopic data are all in excellent agreement with the DFT computations. The reaction outcome upon the chemical reduction of MnInd^{Pyrr} depends on the choice of encapsulating agent, the amount of reductant, and their order of addition. Reduction in the presence of 2,2,2crypt and MnInd^{Pyrr} generated a rare Mn⁰ metalloradical anion that was characterized by X-ray crystallography and EPR spectroscopy, with DFT calculations showing a predominantly metal-based radical character. The reduction of MnInd^{Pyrr} in the absence of the encapsulating agent, followed by the addition of 18-crown-6, results in the formation of an unusual mixed-valent complex in which Mn^I(CO)₃ and Mn^{-I}(CO)₃ moieties are coordinated to a single indenyl ligand. Although the dissociation of the aminoindenyl ligand instead of CO loss diminishes the utility of these compounds as precatalysts for small-molecule activation and electrocatalysis, this study emphasizes that reversible redox activity on the CV time scale does not adequately capture the novel reactivity of indenylmanganate anions in the presence of alkali metal reductants and encapsulating agents.

EXPERIMENTAL SECTION

General Procedures. Compounds were handled under a nitrogen atmosphere in glovebox or via standard Schlenk techniques unless otherwise stated. Commercially available reagents were used as received. Mn(CO)₅Br was either obtained from commercial vendors or synthesized as published.³⁶ Mn(CO)₃(py)₂Br,³⁶ 1-(1*H*-inden-2-yl)-4-methylpiperazine,¹⁴ 1-(1*H*-inden-2-yl)pyrollidine,¹⁶ η ⁵-(2-(*N*methylpiperazine)-indenyl)-manganese tricarbonyl¹⁴ (Ind^{Pip}H), and indenyltricarbonylmanganese¹⁵ (Ind^{Pyrr}H) were also synthesized as published. Potassium graphite (KC₈) was prepared by agitating potassium chunks and graphite flakes at 150 °C under a vacuum.3 The concentration of nBuLi was checked using a quantitative no-D NMR experiment with a 1,5-cyclooctadiene (COD) internal standard.^{38,39} THF used in glovebox work was dried and degassed over alumina columns on a solvent purification system and then stored overnight on 10% w/v molecular sieves before use. 40 Diethyl ether and pentane were dried and degassed over alumina columns on a solvent purification system and directly used without further drying. Solvents used in air-stable reactions were used as received. Column chromatography was performed on silica gel (60 Å, 40-63 μ A, Sorbent Technologies). Celite was heated at 140 °C for several hours and then transferred into a glovebox for use. Infrared spectra were recorded on a Thermo Nicolet FT-IR instrument. Elemental analyses were performed by Atlantic Microlab (Norcross, GA) or the Department of Chemistry at the University of Rochester (Rochester, NY).

NMR. $^{1}\mathrm{H}$ and $^{13}\mathrm{C}$ NMR spectra were collected on a Bruker Avance III 500 MHz NMR with autosampler capability using either a 5 mm BBO broadband ($^{31}\mathrm{P}-^{109}\mathrm{Ag}$, $^{1}\mathrm{H}$, and $^{19}\mathrm{F}$) probe or a 5 mm BBFO broadband ($^{31}\mathrm{P}-^{15}\mathrm{N}$ plus $^{19}\mathrm{F}$ and $^{1}\mathrm{H}$) probe and a 15 mm boron-selective ($^{11}\mathrm{B}$, $^{1}\mathrm{H}$, and $^{19}\mathrm{F}$) probe. $^{55}\mathrm{Mn}$ NMR spectra were obtained on a Bruker Avance III 500 MHz NMR with a 5 mm BBO broadband ($^{31}\mathrm{P}-^{109}\mathrm{Ag}$, $^{1}\mathrm{H}$, and $^{19}\mathrm{F}$) probe at 125 MHz. $^{1}\mathrm{H}$ and $^{13}\mathrm{C}$ NMR spectra were referenced to residual $^{1}\mathrm{H}$ and $^{13}\mathrm{C}$ signals in the deuterated solvent, and $^{55}\mathrm{Mn}$ NMR spectra were referenced externally to a freshly prepared saturated solution of KMnO₄ in D₂O set to 0 ppm. 41,42 Magnetic moments were determined by Evans' method by measuring the paramagnetic shifts of deuterated solvent signals in a known concentration of analyte solution and comparing them with the chemical shift of the deuterated solvent in a flame-sealed capillary tube. 43,44

X-ray Diffraction. Single crystals were mounted on a nylon or Kapton loop and cooled to 100 K under a dry nitrogen stream before data collection unless otherwise stated. SCXRD was performed on a Rigaku XtaLAB Synergy-I diffractometer with a HyPIX HPC detector using Cu $K\alpha$. Structures were refined by full-matrix least-squares based on F2 with all reflections (SHELXTL VS.10; G. Sheldrick, Siemens XRD, Madison, WI). Non-hydrogen atoms were refined with anisotropic displacement coefficients, and hydrogen atoms were treated as idealized contributions. The SADABS (Sheldrick, 12 G.M. SADABS (2.01), Bruker/Siemens Area Detector Absorption Correction Program, Bruker AXS, Madison, WI, 1998) absorption correction was applied. Crystallographic data have been deposited with the Cambridge Crystallographic Data Center and are available free of charge through the CCDC online database.

EPR Spectroscopy. Continuous-wave X-band (9.43898 GHz) EPR spectra were collected at 77 K using a Bruker EMXPlus EPR spectrometer with a standard high-sensitivity X-band resonator. Concentrated solutions were suspended in a frozen 2-MeTHF glass and contained in 4 mm OD quartz tubes. The microwave power was typically 0.2 mW. The field was swept by 1000 G centered at 3400 G and modulated at 100 kHz with 4 G amplitude. A time constant of 20.48 ms was used. Spectra were simulated using EasySpin. 45

Electrochemistry. Cyclic voltammetry experiments were conducted under N_2 at 295 ± 3 K using a standard three-electrode setup consisting of a PEEK-encased glassy carbon working electrode ($\emptyset=1$ mm) and type 2 graphite rod counter electrode ($\emptyset=3$ mm). The Ag/AgCl pseudoreference electrode was stored in a glass compartment containing the solvent and the electrolyte and was separated from the bulk solution using a porous glass frit (Coralpor). The working electrode was polished in the glovebox with 0.25 μ m diamond polishing paste (Buehler) and lapping oil and thoroughly rinsed with the solvent used in the corresponding experiment. A Gamry Reference 1010B potentiostat and Gamry software were used for data collection and analysis, respectively. Samples contained 0.1 M ["Bu₄N][PF₆], organic solvent (3 mL), and 1.0 mM analyte. All CVs are referenced to the Cp₂Fe^{+/0} redox couple (0 V).

DFT Calculations. DFT geometry optimizations and frequency calculations were performed with TURBOMOLE ver. 7.5.1⁴⁶ at the ωB97X-V/def2-TZVP+COSMO(MeCN) level of theory. To reduce the errors from the harmonic approximation, the frequencies were scaled by a factor of 0.95.⁴⁷ Single-point energy calculations on a higher level of theory were performed employing ORCA ver. 5.0.3⁴⁸ with the optimal-tuned (OT)⁴⁹ ωB97X-V functional (see the SI for details) and the large ma-def2-QZVPP basis set. Thermostatistical corrections were obtained from the calculated frequencies via the modified rigid-rotor-harmonic-oscillator scheme, ⁵⁰ and the solvation free energy for the final energy evaluation was obtained with COSMO-RS. For the calculation of reduction potentials, the Cp₂Fe^{+/0} reference was explicitly calculated at the same level of theory.

MnInd^{Pyrr}. 1-(1*H*-Inden-2-yl)pyrollidine (995 mg, 5.37 mmol) was dissolved in THF (25 mL), cooled to -78 °C, and deprotonated with 2.5 M *n*BuLi (2.2 mL, 6 mmol, 1.1 equiv). The brown solution turned red and was warmed to room temperature, forming a suspension. This mixture was reacted at room temperature for 1 h, then Mn(CO)₅Br (1.48 g, 5.37 mmol) was added as a solid under a positive flow of

nitrogen. Upon addition, the solution became dark orange. This solution was then stirred at room temperature for three days. The solvent was then removed in vacuo and purified by silica gel column chromatography (3 cm × 30 cm column) under air. A 1:10 ethyl acetate/hexane mobile phase eluted a small yellow band (Mn₂(CO)₁₀), followed by a larger orange product band. The yellow band was identified to be Mn₂(CO)₁₀ by unit cell analysis via SCXRD (formed by cooling a concentrated pentane solution to -35 °C). The orange solution was not air-stable at room temperature for prolonged periods of time. As soon as the solution was isolated, the solvent was removed on a rotary evaporator, and the product was recrystallized from hexanes in a standard laboratory freezer at −16 °C. The crystalline product was air stable enough to dry and isolate on the benchtop (449 mg, 26%). The resultant crystals were suitable for SCXRD. ¹H NMR (500 MHz, CDCl₃) δ 7.44 (dd, J = 6.6, 3.2 Hz, 2H, H11, H12), 7.01 (dd, J = 6.6, 3.1 Hz, 2H, H10, H13), 4.57 (s, 2H, H6, H9), 3.09-3.03 (m, 4H, H1, H4), 1.97-1.90 (m, 4H, H2, H3). ¹³C NMR (126 MHz, CDCl₃) δ 25.14, 48.84, 55.56, 76.75, 77.00, 77.25, 99.60, 124.90, 125.38, 133.08, 208.30, 225.41. IR (cm⁻¹ KBr) 2957(w), 2923(w), 2852(w), 1989 (s, CO), 1890(s, CO), 1539(s), 1520(m), 1479(m), 1459(m), 1449(m), 1374(w), 1351(w), 1260(w), 1205(w), 1168(w), 1152(m), 1139(m), 1114(w), 1021(w), 993(w), 898(w), 815(m), 798(m), 738(s), 665(s). Elemental Analysis calculated (%) for $C_{16}H_{14}MnNO_3$: C 59.45, H 4.37, : 4.33. Found (%): C 59.48, H 4.39, N 4.44.

[K(18-crown-6)(THF)₂][Mn₂Ind^{Pyrr}]. To a yellow solution of MnInd^{Pyrr} (51.8 mg, 0.160 mmol) in THF (3 mL), KC₈ (45.5 mg, 0.337 mmol) suspended in 1 mL of THF was added dropwise. The reaction mixture was stirred in a 20 mL scintillation vial for 2 h and then filtered through a pad of Celite. To this orange-red solution was added 18-crown-6 (84.7 mg, 0.321 mmol) and the mixture was allowed to stir for 30 min. The solvent was then removed in vacuo, and the resulting dark orange oily solid was washed with diethyl ether (3 × 6 mL) and dried in vacuo. The product yield (82%) was determined by ¹H NMR using 1,3,5-trimethoxybenzene as an internal standard (8.1 mg, 0.048 mmol) along with varying amounts of [K(18crown-6)][Ind^{Pyrr}], which was independently synthesized but had to be accounted for in microanalysis (see below). Crystallization of the crude reduction mixture via pentane vapor diffusion into a concentrated THF solution resulted in dark orange-red crystals suitable for XRD. ¹H NMR (500 MHz, THF) δ 5.79 (dd, J = 5.0, 2.8Hz, 2H, H11, H12), 3.62 (s, 2H, H6, H9), 2.70 (td, J = 5.2, 3.0 Hz, 4H, H1, H4), 1.86 (d, J = 2.8 Hz, 2H, H 10, H13), 1.75 (m, 4H, H2, H3). IR (cm⁻¹, KBr) 2961 (m), 2887 (m), 2824 (m), 1972 (m), 1942 (s), 1857 (s), 1832 (m), 1584 (w), 1457 (w), 1352 (m), 1285 (w), 1258 (w), 1107 (s), 962 (m). Elemental Analysis calculated (%) for $[C_{31}H_{38}NO_{12}Mn_2K] \cdot [C_{25}H_{38}NO_6K]_{0.7} \colon \ C \ 52.62, \ H \ 5.88, \ N \ 2.15.$ Found (%): C 52.92, H 6.18, N 1.97

[K(18-crown-6)][Mn_2Ind^{pyrr}]. The ether washings of the crystal-lized $[K(18\text{-crown-6})(THF)_2][Mn_2Ind^{pyrr}]$ were concentrated and then cooled at -35 °C for several days, leading to milligram quantities of the THF-free adduct $[K(18\text{-crown-6})][Mn_2Ind^{pyrr}]$ that were suitable for X-ray diffraction. The yield was not determined.

[K(2,2,2-Crypt)][Ind^{Pyrr}]. To a stirred yellow solution of Ind^{Pyrr}H (49.7 mg, 0.154 mmol) and 2,2,2-Crypt (142 mg, 0.397 mmol) in THF (3 mL) in a 20 mL scintillation vial, KC₈ (55.9 mg, 0.414 mmol) suspended in a 1 mL THF solution was added dropwise. The solution was stirred for 1 h at room temperature and then filtered through a pad of Celite. The solution was concentrated to ca. 2 mL and then stored overnight at -35 °C, resulting in the crystallization of the product. The solvent was then decanted and the crystals were dried in vacuo, yielding analytically pure [K(2,2,2-Crypt)][Ind^{Pyrr}] (88 mg, 96%). ¹H NMR (500 MHz, THF) δ 6.84 (dd, I = 5.7, 3.1 Hz, 2H), 6.05 (dd, *J* = 5.7, 3.0 Hz, 2H), 5.21 (s, 2H), 3.26 (s, 12H), 3.20 (t, J = 4.7 Hz, 12H), 3.18-3.13 (m, 4H), 2.25-2.20 (m, 12H), 1.90-1.81 (m, 4H). 13 C NMR (126 MHz, THF) δ 26.03, 51.13, 54.72, 68.35, 71.06, 79.94, 109.40, 114.99, 131.77, 148.54. IR (cm-1, KBr) 2961 m, 2873 m, 2813 m, 1587 s, 1462 m, 1358 s, 1291 w, 1258 w, 1126 m, 1099 s, 948 m, 933 m. Elemental Analysis calculated (%) for

 $\rm C_{31}H_{50}KN_3O_6$: C 62.07, H 8.40, N 7.01. Found (%): C 62.25, H 8.09, N 6.79.

[K(2,2,2-Crypt)][MnInd^{Pyrr}]. To a stirred yellow solution of MnInd^{Pyrr} (37 mg, 0.11 mmol) and 2,2,2-Crypt (43 mg, 0.11 mmol) in THF (3 mL) in a 20 mL scintillation vial, KC₈ (17 mg, 0.13 mmol) suspended in a 1 mL THF solution was added dropwise . The mixture was stirred for 2 h and then filtered through a pad of Celite. The solvent was concentrated to ca. 0.5 mL, and the resulting deep green solution was diluted with diethyl ether. The solvent was removed in vacuo, during which the product crystallized as dark green needles. These crystals were washed with diethyl ether, then dried under high vacuum to generate the product (31 mg, 36%) and a nearly equimolar amount of $[K(2,2,2-Crypt)][Mn(CO)_5]$ (0.7 equiv) as determined by elemental analysis. Crystals suitable for XRD were grown via pentane vapor diffusion into a concentrated THF solution of [K(2,2,2-Crypt)][MnInd^{Pyrr}] that also contained colorless crystals of $[K(2,2,2-Crypt)][Mn(CO)_5]$. IR (cm^{-1}, KBr) 2965 w, 2888 w, 2819 w, 1884 s (CO), 1807 m (CO), 1784 m (CO), 1547 w, 1511 w, 1480 w, 1445 w, 1355 m, 1297 w, 1260 w, 1170 w, 1133 m, 1102 s, 950 m, 933 m. Elemental Analysis calculated (%) fir $[C_{34}H_{53}N_3O_9MnK]\cdot [C_{23}H_{36}N_2O_{11}MnK]_{0.7}\!\!: C$ 51.46, H 6.74, N 5.27. Found (%): C 51.83, H 6.28, N 5.04. Magnetic moment: μ_{eff} = 1.69 $\mu_{\rm B}$ (THF- $d_{\rm 8}$).

ASSOCIATED CONTENT

Solution Supporting Information

The Supporting Information is available free of charge at https://pubs.acs.org/doi/10.1021/acs.organomet.2c00463.

Computed Cartesian coordinates (XYZ)
Electrochemistry, molecular structures, NMR spectra, IR spectra, and DFT computational workflow (PDF)

Accession Codes

CCDC 2202042 and 2202047–2202051 contain the supplementary crystallographic data for this paper. These data can be obtained free of charge via www.ccdc.cam.ac.uk/data_request/cif, or by emailing data_request@ccdc.cam.ac.uk, or by contacting The Cambridge Crystallographic Data Centre, 12 Union Road, Cambridge CB2 1EZ, UK; fax: +44 1223 336033.

AUTHOR INFORMATION

Corresponding Authors

Demyan E. Prokopchuk — Department of Chemistry, Rutgers University—Newark, Newark, New Jersey 07102, United States; Occid.org/0000-0002-6352-3509; Email: demyan.prokopchuk@rutgers.edu

Andreas Hansen – Mulliken Center for Theoretical Chemistry, Clausius-Institut für Physikalische und Theoretische Chemie, Rheinische Friedrich-Wilhelms Universität Bonn, Bonn 53115, Germany; orcid.org/0000-0003-1659-8206; Email: hansen@thch.uni-bonn.de

Authors

David S. Tresp − Department of Chemistry, Rutgers University—Newark, Newark, New Jersey 07102, United States; ocid.org/0000-0003-4743-6269

Hagen Neugebauer – Mulliken Center for Theoretical Chemistry, Clausius-Institut für Physikalische und Theoretische Chemie, Rheinische Friedrich-Wilhelms Universität Bonn, Bonn 53115, Germany; orcid.org/0000-0003-1309-0503

Stefan Grimme – Mulliken Center for Theoretical Chemistry, Clausius-Institut für Physikalische und Theoretische Chemie, Rheinische Friedrich-Wilhelms Universität Bonn, Bonn 53115, Germany; orcid.org/0000-0002-5844-4371

Complete contact information is available at: https://pubs.acs.org/10.1021/acs.organomet.2c00463

Notes

The authors declare no competing financial interest.

ACKNOWLEDGMENTS

D.S.T. thanks Prof. Roger Lalancette at Rutgers—Newark for instruction in collecting, refining, and solving crystallographic data. D.E.P. and D.T. thank Prof. Donald J. Hirsh at The College of New Jersey for EPR spectrometer access, Dr Pavel Kucheryavy at Rutgers—Newark for assistance with ⁵⁵Mn NMR spectroscopy, and Dr. Alexei Tyryshkin at Rutgers—New Brunswick for EPR simulations and insights. D.E.P. thanks the National Science Foundation (NSF) for support under Grant 2055097, and S.G. thanks the Deutsche Forschungsgemeinschaft under Grant 1927/16-1. X-ray structural data were supported by the NSF under Grant 2018753, and this research was supported in part by a Rutgers University—Newark startup grant (D.E.P.).

REFERENCES

- (1) Appel, A. M.; DuBois, D. L.; Rakowski DuBois, M. Molybdenum-Sulfur Dimers as Electrocatalysts for the Production of Hydrogen at Low Overpotentials. *J. Am. Chem. Soc.* **2005**, 127 (36), 12717–12726.
- (2) Artero, V.; Fontecave, M. Hydrogen evolution catalyzed by {CpFe(CO)₂}-based complexes. *Comptes Rendus Chimie* **2008**, *11* (8), 926–931.
- (3) Waldie, K. M.; Kim, S.-K.; Ingram, A. J.; Waymouth, R. M. Cyclopentadienyl Cobalt Complexes as Precatalysts for Electrocatalytic Hydrogen Evolution. *Eur. J. Inorg. Chem.* **2017**, 2017 (20), 2755–2761.
- (4) Goh, Y. X. C.; Tang, H. M.; Loke, W. L. J.; Fan, W. Y. Bis(cyclopentadienyl)nickel(II) μ -Thiolato Complexes as Proton Reduction Electrocatalysts. *Inorg. Chem.* **2019**, 58 (18), 12178–12183.
- (5) Sánchez, P.; Goel, B.; Neugebauer, H.; Lalancette, R. A.; Grimme, S.; Hansen, A.; Prokopchuk, D. E. Ligand Protonation at Carbon, not Nitrogen, during H₂ Production with Amine-Rich Iron Electrocatalysts. *Inorg. Chem.* **2021**, *60* (22), 17407–17413.
- (6) Gonell, S.; Miller, A. J. M. Chapter One Carbon Dioxide Electroreduction Catalyzed by Organometallic Complexes. In *Advances in Organometallic Chemistry*, Vol. 70; Pérez, P. J., Stone, F. G. A., West, R., Eds.; Academic Press, 2018; pp 1–69.
- (7) Rosas-Hernández, A.; Junge, H.; Beller, M.; Roemelt, M.; Francke, R. Cyclopentadienone iron complexes as efficient and selective catalysts for the electroreduction of CO₂ to CO. *Catalysis Science & Technology* **2017**, 7 (2), 459–465.
- (8) Drover, M. W.; Schild, D. J.; Oyala, P. H.; Peters, J. C. Snapshots of a Migrating H-Atom: Characterization of a Reactive Iron(III) Indenide Hydride and its Nearly Isoenergetic Ring-Protonated Iron(I) Isomer. *Angew. Chem., Int. Ed.* **2019**, 58 (43), 15504–15511.
- (9) Laws, D. R.; Chong, D.; Nash, K.; Rheingold, A. L.; Geiger, W. E. Cymantrene Radical Cation Family: Spectral and Structural Characterization of the Half-Sandwich Analogues of Ferrocenium Ion. J. Am. Chem. Soc. 2008, 130 (30), 9859–9870.
- (10) Wu, K.; Laws, D. R.; Nafady, A.; Geiger, W. E. Substitution of CO Ligand by $P(OPh)_3$ in Radical Cations of the Cymantrene Family: Relationships of Substitution Rates to $E^{1/2}$ Values and Carbonyl IR Frequencies. *J. Inorg. Organomet. Polym Mater.* **2014**, 24 (1), 137–144.
- (11) Sawtelle, S. M.; Johnston, R. F.; Cook, C. C. An investigation of electron transfer properties of (Cp)Mn(CO)₃ and substituted Cp derivatives. *Inorg. Chim. Acta* **1994**, *221* (1), 85–92.
- (12) Lee, S.; Lovelace, S.; Cooper, N. J. Two-Electron and One-Electron Reduction of the Indenyl Complex $[Mn(\eta^5-C_9H_7)(CO)_3]$

- and Reversible Counterion-Controlled Comproportionation of [Mn- $(\eta^5\text{-C}_9\text{H}_7)(\text{CO})_3$] and [Mn $(\eta^3\text{-C}_9\text{H}_7)(\text{CO})_3$]²⁻ To Give [Mn $(\eta^5\text{-C}_9\text{H}_7)(\text{CO})_3$]. Organometallics **1995**, 14 (4), 1974–1982.
- (13) Pevear, K.; Holl, M. B.; Carpenter, G.; Rieger, A.; Rieger, P.; Sweigart, D. Ligand Substitution at 19-Electron Centers and the Indenyl Effect in Organometallic Radicals. Electrocatalytic CO Substitution in (cyclopentadienyl) Fe (CO) ³⁺ and (indenyl) Fe (CO) ³⁺. Organometallics 1995, 14 (1), 512–523.
- (14) Plenio, H.; Burth, D. Syntheses and X-Ray Crystal Structures of 2-Aminoindenes and Aminocymantrenes. Z. Anorg. Allg. Chem. 1996, 622 (2), 225–230.
- (15) King, R. B.; Efraty, A. Organometallic chemistry of the transition metals XXIII. Some indenyl and fluorenyl derivatives of manganese carbonyl. *J. Organomet. Chem.* 1970, 23 (2), 527–533.
- (16) Rufanov, K. A.; Titov, I. Y.; Lemenovskii, D. A.; Krut'ko, D. P.; Churakov, A. V. Novel approach for the synthesis of chiral organometallic complexes first series of lithium 2-amino-indenide ligands bearing pendant donor groups and a unique helical bent-zirconocene. *New J. Chem.* **2022**, *46* (3), 1409–1415.
- (17) Bursch, M.; Mewes, J.-M.; Hansen, A.; Grimme, S. Best Practice DFT Protocols for Basic Molecular Computational Chemistry. *Angew. Chem., Int. Ed.* **2022**, *61*, e202205735.
- (18) Mardirossian, N.; Head-Gordon, M. ω B97X-V: A 10-parameter, range-separated hybrid, generalized gradient approximation density functional with nonlocal correlation, designed by a survival-of-the-fittest strategy. *Phys. Chem. Chem. Phys.* **2014**, *16* (21), 9904–9924.
- (19) Klamt, A.; Schüürmann, G. COSMO: a new approach to dielectric screening in solvents with explicit expressions for the screening energy and its gradient. *J. Chem. Soc., Perkin Trans.* 2 **1993**, No. 5, 799–805.
- (20) Weigend, F.; Ahlrichs, R. Balanced basis sets of split valence, triple zeta valence and quadruple zeta valence quality for H to Rn: Design and assessment of accuracy. *Phys. Chem. Chem. Phys.* **2005**, 7 (18), 3297–3305.
- (21) Allen, F. H.; Kennard, O.; Watson, D. G.; Brammer, L.; Orpen, A. G.; Taylor, R. Tables of bond lengths determined by X-ray and neutron diffraction. Part 1. Bond lengths in organic compounds. *J. Chem. Soc., Perkin Trans.* 2 **1987**, No. 12, S1–S19.
- (22) Geiger, W. E. One-electron electrochemistry of parent pianostool complexes. *Coord. Chem. Rev.* **2013**, 257 (9), 1459–1471.
- (23) Salmain, M.; Jaouen, G.; Fiedler, J.; Sokolová, R.; Pospíšil, L. Mechanism of Reduction of Cymantrene (Tricarbonyl η^5 -Cyclopentadienylmanganese) and Its Methyl Carboximidate Derivative. *Collect. Czech. Chem. Commun.* **2001**, *66*, 155–169.
- (24) Zheng, J.; Xu, X.; Truhlar, D. G. Minimally augmented Karlsruhe basis sets. *Theor. Chem. Acc.* **2011**, *128* (3), 295–305.
- (25) Klamt, A. Conductor-like screening model for real solvents: a new approach to the quantitative calculation of solvation phenomena. *J. Phys. Chem.* **1995**, 99 (7), 2224–2235.
- (26) Klamt, A.; Jonas, V.; Bürger, T.; Lohrenz, J. C. Refinement and parametrization of COSMO-RS. J. Phys. Chem. A 1998, 102 (26), 5074–5085.
- (27) Ellis, J. E.; Flom, E. A. The chemistry of metal carbonyl anions: III. Sodium-potassium alloy: An efficient reagent for the production of metal carbonyl anions. *J. Organomet. Chem.* **1975**, *99* (2), 263–268.
- (28) Masters, A. P.; Sorensen, T. S. Pentacarbonylmanganese enolate and dienolate complexes. Preparative and mechanistic considerations. *Can. J. Chem.* **1990**, *68* (3), 492–501.
- (29) Narro, A. L.; Arman, H. D.; Tonzetich, Z. J. Manganese Chemistry of Anionic Pyrrole-Based Pincer Ligands. *Organometallics* **2019**, 38 (8), 1741–1749.
- (30) Cheng, J.; Chen, Q.; Leng, X.; Ouyang, Z.; Wang, Z.; Ye, S.; Deng, L. The Stabilization of Three-Coordinate Formal Mn(0) Complex with NHC and Alkene Ligation. *Chem.* **2018**, *4* (12), 2844–2860.
- (31) Sampson, M. D.; Nguyen, A. D.; Grice, K. A.; Moore, C. E.; Rheingold, A. L.; Kubiak, C. P. Manganese Catalysts with Bulky Bipyridine Ligands for the Electrocatalytic Reduction of Carbon

Dioxide: Eliminating Dimerization and Altering Catalysis. J. Am. Chem. Soc. 2014, 136 (14), 5460–5471.

- (32) Agnew, D. W.; Moore, C. E.; Rheingold, A. L.; Figueroa, J. S. Kinetic Destabilization of Metal-Metal Single Bonds: Isolation of a Pentacoordinate Manganese(0) Monoradical. *Angew. Chem., Int. Ed.* **2015**, *54* (43), 12673–12677.
- (33) Karagiannis, A.; Tyryshkin, A. M.; Lalancette, R. A.; Spasyuk, D. M.; Washington, A.; Porkopchuk, D. E. A Redox-Active Mn(0) Dicarbene Metalloradical. *Chem. Commun.* **2022**, DOI: 10.1039/D2CC04677F.
- (34) Brousses, R.; Maurel, V.; Mouesca, J.-M.; César, V.; Lugan, N.; Valyaev, D. A. Half-sandwich manganese complexes Cp(CO)2Mn(NHC) as redox-active organometallic fragments. *Dalton Trans.* **2021**, 50 (40), 14264–14272.
- (35) Kudinov, A. R.; Petrovskii, P. V.; Struchkov, Y. T.; Yanovskii, A. I.; Rybinskaya, M. I. Synthesis of slipped triple- and tetra-decker cationic ruthenium complexes with the μ , η^5 : η^6 -indenyl ligand. X-Ray structure of $[(\eta-C_5H_5)Ru(\mu, \eta^5: \eta^6-C_9H_7-Ru(\eta-C_5Me_5)]PF_6$. J. Organomet. Chem. **1991**, 421 (1), 91–115.
- (36) Abel, E.; Wilkinson, G. 291. Carbonyl halides of manganese and some related compounds. *J. Chem. Soc.* **1959**, 1501–1505.
- (37) Rodriguez, M. M.; Bill, E.; Brennessel, W. W.; Holland, P. L. N_2 Reduction and Hydrogenation to Ammonia by a Molecular Iron-Potassium Complex. *Science* **2011**, 334, 780–783.
- (38) Hoye, T. R.; Eklov, B. M.; Ryba, T. D.; Voloshin, M.; Yao, L. J. No-D NMR (No-Deuterium Proton NMR) Spectroscopy: A Simple Yet Powerful Method for Analyzing Reaction and Reagent Solutions. *Org. Lett.* **2004**, *6* (6), 953–956.
- (39) Hoye, T. R.; Eklov, B. M.; Voloshin, M. No-D NMR Spectroscopy as a Convenient Method for Titering Organolithium (RLi), RMgX, and LDA Solutions. *Org. Lett.* **2004**, *6* (15), 2567–2570
- (40) Williams, D. B. G.; Lawton, M. Drying of Organic Solvents: Quantitative Evaluation of the Efficiency of Several Desiccants. *J. Org. Chem.* **2010**, 75 (24), 8351–8354.
- (41) Fulmer, G. R.; Miller, A. J. M.; Sherden, N. H.; Gottlieb, H. E.; Nudelman, A.; Stoltz, B. M.; Bercaw, J. E.; Goldberg, K. I. NMR Chemical Shifts of Trace Impurities: Common Laboratory Solvents, Organics, and Gases in Deuterated Solvents Relevant to the Organometallic Chemist. *Organometallics* **2010**, *29* (9), 2176–2179.
- (42) Lutz, O.; Steinkilberg, W. ⁵⁵Mn NMR Studies in Aqueous Permanganate Solutions. Z. Naturforsch. A **1974**, 29 (10), 1467–1470.
- (43) Evans, D. F. 400. The determination of the paramagnetic susceptibility of substances in solution by nuclear magnetic resonance. *J. Chem. Soc.* **1959**, No. 0, 2003–2005.
- (44) Sur, S. K. Measurement of magnetic susceptibility and magnetic moment of paramagnetic molecules in solution by high-field fourier transform NMR spectroscopy. *J. Magn. Reson.* **1989**, 82 (1), 169–173.
- (45) Stoll, S.; Schweiger, A. EasySpin, a comprehensive software package for spectral simulation and analysis in EPR. *J. Magn. Reson.* **2006**, *178* (1), 42–55.
- (46) TURBOMOLE, ver. 7.5.1; TURBOMOLE GmbH: Karlsruhe, Germany, 2021. https://www.turbomole.org.
- (47) Kesharwani, M. K.; Brauer, B.; Martin, J. M. L. Frequency and Zero-Point Vibrational Energy Scale Factors for Double-Hybrid Density Functionals (and Other Selected Methods): Can Anharmonic Force Fields Be Avoided? *J. Phys. Chem. A* **2015**, *119* (9), 1701–1714.
- (48) Neese, F. Software update: The ORCA program system, version 4.0. WIREs Comput. Mol. Sci. 2018, 8 (1), No. e1327.
- (49) Baer, R.; Livshits, E.; Salzner, U. Tuned range-separated hybrids in density functional theory. *Annu. Rev. Phys. Chem.* **2010**, *61*, 85–109.
- (50) Grimme, S. Supramolecular binding thermodynamics by dispersion-corrected density functional theory. *Chem. Eur. J.* **2012**, 18 (32), 9955–9964.

□ Recommended by ACS

Impact of Counteranion on Reversible Spin-State Switching in a Series of Cobalt(II) Complexes Containing a Redox-Active Ethylenedioxythiophene-Based Terpyridine Ligand

Subrata Ghosh, Abhishake Mondal, et al.

OCTOBER 20, 2022 INORGANIC CHEMISTRY

READ 🖸

Interplay between β -Diimino and β -Diketiminato Ligands in Nickel Complexes Active in the Proton Reduction Reaction

Navid Jameei Moghaddam, Antoni Llobet, et al.

OCTOBER 05, 2022

INORGANIC CHEMISTRY

READ 🗹

Constructing "Closed" and "Open" {Mn₈} Clusters

Thomais G. Tziotzi, Constantinos J. Milios, et al.

JULY 05. 2022

CRYSTAL GROWTH & DESIGN

READ 🗹

55/52Mn²⁺ Complexes with a Bispidine-Phosphonate Ligand: High Kinetic Inertness for Imaging Applications

Maryame Sy, Aline M. Nonat, et al.

AUGUST 19, 2022

INORGANIC CHEMISTRY

READ **C**

Get More Suggestions >